On the Molecular Mechanism of H_2O Diffusion into Polyimides: A Vibrational Spectroscopy Investigation

Pellegrino Musto,*,† Giuseppe Ragosta,† Giuseppe Mensitieri,‡ and Marino Lavorgna§

Institute of Chemistry and Technology of Polymers, National Research Council of Italy, Via Campi Flegrei, 34, 80078, Pozzuoli (Naples), Italy, Department of Materials and Production Engineering, University of Naples Federico II, P.le Tecchio 80, 80125, Naples, Italy, Institute of Composite and Biomedical Materials, National Research Council of Italy, Piazzale Tecchio 80, 80125, Naples, Italy

Received June 21, 2007; Revised Manuscript Received September 25, 2007

ABSTRACT: The diffusion of water into polyimide films was studied by in situ FTIR spectroscopy using several methods of spectral data analysis, namely, difference spectroscopy, least-squares curve fitting, 2D correlation spectroscopy, and normal coordinate analysis. The results gave an insight into the molecular mechanism of diffusion in terms of number and population of penetrant species present in the system and with respect to the nature of the molecular aggregates. In particular, two water species were identified and quantified, i.e., H_2O molecules interacting with the carbonyl groups of the polyimide and self-associated water. An enthalpy of formation of -0.9 kcal mol^{-1} was estimated for the H_2O−polyimide interaction, which points to a relatively weak H-bonding tendency of the imide carbonyls. Finally, the infrared spectrum of the H_2O−imide aggregate was calculated by a quantum mechanic (QM) model chemistry to rationalize the effects observed in the spectrum of the water saturated films. The results of the computation were in good agreement with the experiment, confirming the predictive capabilities of the chosen QM method and supporting the proposed molecular structure of the H-bonding aggregate.

Introduction

Polyimides are a well-known class of high-performance technopolymers characterized by outstanding properties in terms of thermal-oxidative stability, mechanical performances, high glass-transition temperature (T_g), and good resistance to solvents.[1−4] These properties make them attractive for microelectronic and optoelectronic applications and as membranes for separation technologies.[5−8] More recently, several polyimides have been employed as polymeric components of high-performance hybrid systems, prepared via the sol−gel route.[9−12]

The polyimides and even more so, the hybrid materials prepared therefrom, exhibit interesting peculiarities in connection to their sorption properties.[10−12] In particular, the diffusion of water has obvious implications on the behavior of these materials, especially in microelectronic applications where absorbed moisture may cause reliability problems such as increase in dielectric constant, metal corrosion of devices, loss of adhesion, and mechanical failures.[13−15] Water diffusion in polyimides has been shown to be a complex process[14−17] whose mechanism is still poorly understood at a molecular level. This state of affairs is not limited to this class of polymers, but is a rather general one, as pointed out by Marechal in a recent review article.[18]

Despite the lack of generally accepted knowledge, the importance taken by H_2O molecules when embedded in macromolecular systems cannot be overestimated. This is not only true in biosystems where the crucial role of water has been recognized for long but is becoming more and more apparent even in the realm of synthetic polymers. An increase of interest has therefore occurred on the subject, witnessed by the many studies that have recently appeared in the literature (see, for instance, those on the hydration mechanism of ionomer membranes to be used in fuel-cell technology[19−22]). The issues to be addressed when attempting a molecular level description of a polymer−water system are manyfold: water is the only molecule possessing two acceptor and two donor sites for hydrogen bonding, which gives it the possibility to suddenly change the interaction configuration according to the surrounding environment and accounts for its ubiquitous character and versatility. This same property, however, makes water molecules rather difficult to observe. Even the more sensitive method for H-bonding detection, i.e., IR spectroscopy, is plagued by limited resolution, due to the considerable band broadening in the ν_{OH} range. Another weakness of the IR technique is represented by the intensity enhancement of the ν_{OH} bands, upon the establishment of the interaction.[18,19,23] This poorly predictable effect contributes to complicate the quantitative analysis in terms of the population of interacting species, although several approaches have been proposed in the literature to overcome this problem.[18,19,23−25]

Whenever the amount of water absorbed at equilibrium is conspicuous (10% by weight or more), it happens that the hydration mechanism is dependent on the overall water content in the sample. Thus, both the interactions with the polymer substrate and the self-association of the penetrant molecules change in going from the early stages of the sorption process onward. Clearly, in these instances, which are often the most relevant from an application perspective, the situation is even more complicated but still amenable to, at least, a semiquantitative analysis.[18,19,24] Several approaches have been proposed in recent years to fully exploit the molecular level information contained in the vibrational spectrum. In particular, the methods developed by Marechal[18,19,24] have clearly established IR spectroscopy as one of the most powerful techniques to investigate water molecules in macromolecular environments

* Corresponding author. E-mail: musto@ictp.cnr.it.
† Institute of Chemistry and Technology of Polymers, National Research Council of Italy.
‡ University of Naples Federico II.
§ Institute of Composite and Biomedical Materials, National Research Council of Italy.

10.1021/ma071385+ CCC: $37.00
Published on Web 11/08/2007

Chart 1

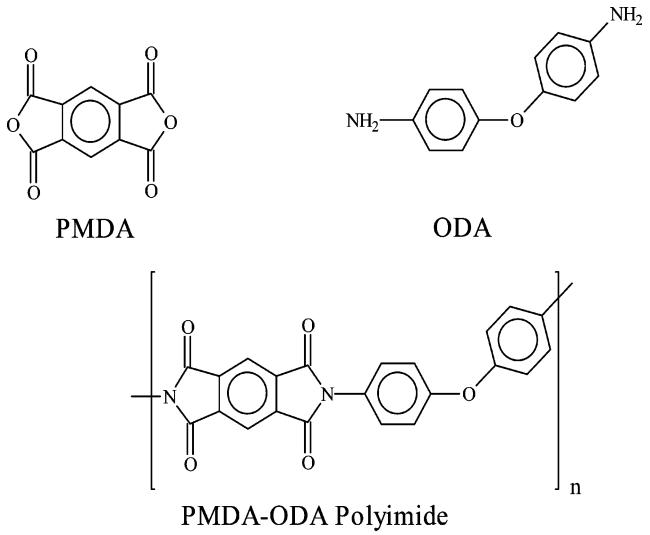

and have considerably contributed to the advancement of our fundamental understanding of water diffusion phenomena.

Among the available techniques, we may cite least-squares curve fitting, Fourier self-deconvolution, difference spectroscopy, and 2D-FTIR correlation spectroscopy. In particular, the latter technique offers a number of distinct advantages in connection with complex, extensively overlapped spectral profiles, as are those relative to water absorbed in interacting media. The appealing features of the 2D-FTIR approach are the following: (i) it may improve the resolution, thus revealing the fine structure of otherwise unresolved profiles; (ii) it can aid in the identification of the distinct molecular species present in the system and the signals they produce; (iii) it may provide information about the dynamics of the system making use of the asynchronous spectral information.[26]

In the present contribution, the FTIR spectra collected in situ during the sorption−desorption cycle of water in polyimide are examined by means of difference spectroscopy, curve-resolving analysis, and 2D-FTIR correlation spectroscopy. The above approaches provide relevant and complementary information about the transport process, in terms of overall diffusivity, molecular interactions among the penetrant and the substrate, and dynamics of the different molecular species present into the investigated system. The last part of the contribution is devoted to the theoretical calculation of the infrared spectrum of the water−polyimide aggregate, aimed at a deeper understanding of its molecular structure.

Experimental Section

Materials. The polyimide precursor used in this study was a polyamic acid, Pyre-ML RK 692, from I.S.T (Indian Orchard, MA). This has molecular weights $\bar{M}_w = 1.0 \times 10^5$ and $\bar{M}_n = 4.6 \times 10^4$ and is supplied as a 12 wt % solution in a mixture of *N*-methyl-2-pyrrolidone (NMP) and xylene (weight ratio 80/20).

The polyamic acid is obtained by condensation of pyromellitic dianhydride (PMDA) and oxidianiline (ODA), whose structures are reported in Chart 1.

Preparation of the Polyimide Films. Castings 20−30 μm thick were obtained by spreading the polyamic acid solution onto a glass plate with the aid of a Gardner knife. The cast films were allowed to dry for 1 h at room temperature and then for 1 h at 80 °C to allow most of the solvent to evaporate. Imidization reactions were carried out in successive isothermal steps of 1 h each at 100, 150, 200, 250, and 300 °C. Finally, the cured films were peeled off from the glass substrate by immersing in distilled water at 80 °C.

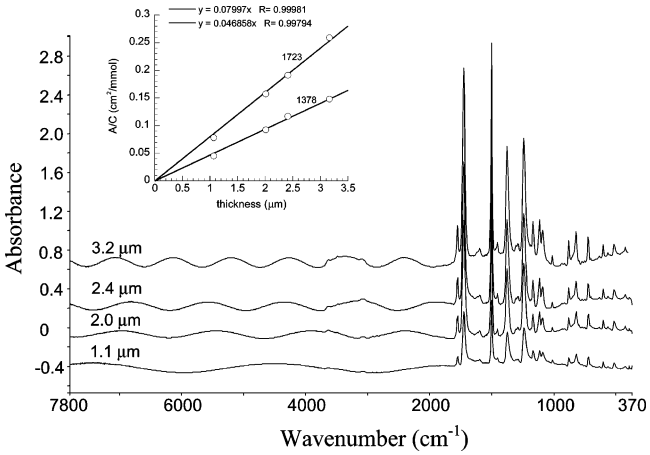

Figure 1. FTIR spectrum in the wavenumber range 7800−370 cm^{-1} for polyimide films of different thickness prepared by the spin-coating technique. Thickness as indicated. The inset displays a Lambert−Beer plot relative to the peaks at 1723 and 1378 cm^{-1}.

Thinner films (3.2−1.0 μm) were obtained by spin-coating a prescribed amount of the polyamic acid solution onto a glass substrate. The spin-coating was a two-step process performed with a Chemat KW-4A apparatus equipped with an automated fluid dispenser (KW-4AD), from Chemat Technologies Inc., Northridge, CA. The spinning conditions were 12 s at 700 rpm for the first step and 20 s at 1500 rpm for the second step. Curing conditions for the spin-coated films were the same as those for the thick films. The spectra collected on different spin-coated films of pure polyimide are reported in Figure 1. The pattern of interference fringes is evident in all cases, which affords a precise determination of the film thickness. This is accomplished by applying the relationship:[27]

$$L = \frac{\Delta n}{2(\nu_2 - \nu_1)\eta} \tag{1}$$

where L is the film thickness, Δn is the number of cycles in the wavenumber range between ν_2 and ν_1, and η is the refractive index of the sample. In the inset of Figure 1 is reported the absorbance/concentration ratio as a function of the film thickness for the two main peaks of the imide ring. The calibration curves, in the form of straight lines passing through the origin, confirm that, in the investigated thickness range, the Beer−Lambert relationship is verified and afford the evaluation of film thickness even in the absence of interference fringes.

Techniques. FTIR Spectroscopy. A vacuum tight FTIR cell was used to record the FTIR transmission spectra of the polymer films exposed to water vapor at constant pressure. The cell was connected through service lines to a water reservoir, a vacuum pump, and pressure transducers. Full details of the experimental setup are reported in refs 28 and 29.

The instrument used for the collection of FTIR spectra was a Spectrum-GX from Perkin-Elmer (Norwalk, CT), equipped with a germanium/KBr beam splitter and a wide-band DTGS detector. The instrumental parameters for data collection were as follows: resolution = 4 cm^{-1}, optical path difference (OPD) velocity = 0.2 cm/s, spectral range = 4000−400 cm^{-1}. A single data collection was performed for each spectrum which took 1.5 s to complete under the chosen instrumental conditions. The signals were acquired as single beam spectra at specific time intervals. A typical sorption run lasted about 30 min, while the acquisition time intervals were 6 s during the first 10 min of the experiment and 60 s thereafter. Automated data acquisition was driven by a dedicated software package for time-resolved spectroscopy (Timebase from Perkin-Elmer).

Sorption−desorption tests were performed at 30 °C and at relative pressures, p/p_0, varying from 0.1 to 0.80 (where p is the experimental pressure and p_0 is the saturation pressure of water vapor at

30 °C, corresponding to 31.8 Torr). The relative pressure was assumed to be equal to the water activity, a_w, in view of the low value of p_0.

FTIR Data Analysis. The complete absorbance spectra (i.e., polyimide plus sorbed water) were obtained using the empty cell as background at the test conditions. Time-resolved spectra of sorbed water were isolated by eliminating the interference caused by the polymer matrix. This was accomplished by using the ratio method:[30] the water spectrum at time t was obtained using the single-beam, transmission spectrum of the dry specimen as background, i.e.,

$$A_t(\upsilon) = \log\frac{I_0(\upsilon)}{I_t(\upsilon)} \tag{2}$$

where $A_t(\upsilon)$ is the absorbance spectrum of the penetrant, $I_0(\upsilon)$ is the single-beam transmission spectrum collected at time = 0 (dry specimen), and $I_t(\upsilon)$ is the single-beam transmission spectrum at time t. It is noted that $A_t(\upsilon)$ corresponds to the subtraction spectrum $A_d(\upsilon)$:

$$A_d(\upsilon) = A_t(\upsilon) - KA_0(\upsilon) \tag{3}$$

for $K = 1$. K is the subtraction factor, i.e., an adjustable parameter used to compensate for possible thickness differences between "wet" and "dry" samples. Subtraction spectroscopy has also been used in connection with the analysis of the carbonyl band shape, in which case the K parameter holds information about concentration ratios. The correspondence between eqs 2 and 3 holds whenever there is a negligible change in volume as a result of penetrant sorption, as in the present case. When this condition is satisfied, eq 2 can be used in place of the more general eq 3. The use of eq 2 is generally preferred as it avoids the problems related to the long-term background instability. The absorbance areas of the subtraction spectra in the ν_{OH} region (3800−3000 cm^{-1}) and in the in-plane bending interval (1680−1570 cm^{-1}) were used to monitor the amount of water present in the sample as a function of time.

In the case of unresolved, multicomponent bands, a curve resolving algorithm based on the Levenberg−Marquardt method was used to separate the individual peaks.[31,32] In order to reduce the number of adjustable parameters, the baseline, the band shape, and the number of components were fixed and the curve-fitting analysis yielded the height, the full width at half-height (FWHH), and the position of the individual components. The minimum number of components was determined by visual inspection and by a second-derivative analysis of the experimental profile. The peak function used throughout was a Gaussian line-shape.[32]

Before the 2D-IR correlation analysis was performed, the experimental spectra were preprocessed to avoid the occurrence of artifacts due to baseline instabilities and other nonselective effects.[33,34] The frequency region of interest (3900−3200 cm^{-1}) was truncated and subjected to a linear baseline correction, followed by offset to zero absorbance. Generalized 2D-IR was performed by a computer program written in house in the Grams/32 environment (Galactic Industries Co., Salem, NH), using the associated programming language Array Basic. A recently developed algorithm was employed, relying on the Hilbert transform,[35] which offers an easier and more efficient method for the numerical evaluation of the correlation intensities.

The 2-D correlation analysis was performed on an evenly spaced sequence of 20 spectra collected at a constant sampling interval of 12 s. It was found that considering shorter time intervals does not improve the quality and resolution of the resulting correlation spectra.

The notation adopted to identify the peaks appearing in the correlation spectra is the following: the x-axis frequency coordinate is written first, followed by the y-axis coordinate, both enclosed in square brackets. Following the coordinate values, a ± sign enclosed in round brackets specifies the positive or negative value of the peak. The sign is omitted for autopeaks, these being always positive. It is explicitly noted that, for concision, only the peaks appearing in the lower side of the spectrum with respect to the diagonal line with coordinates $[\nu_i,\nu_i]$ are referred to, with the understanding that, due to the symmetry of the correlation spectra, corresponding cross-peaks are located in the upper side of the spectrum, at appropriate positions.

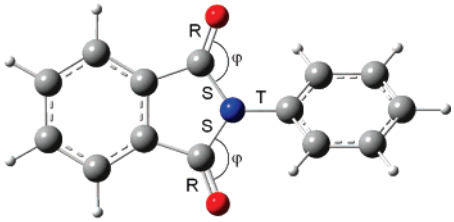

Figure 2. Optimized geometry of *N*-phenylphthalimide. The atoms are represented according to their relative Van der Waals radii. Atoms' color code: white = H; gray = C; red = O, blue = N. In the figure are also represented the internal coordinates contributing to the Potential Energy Distribution of the normal modes reported in Table IV. R, S, T = stretching coordinates; φ = in-plane bending coordinates.

Gravimetric Analysis. The equipment used to determine the weight gain of samples exposed to a controlled humidity environment is similar to that used for the on-line FTIR spectroscopy measurements. In place of the FTIR measuring cell, an electronic microbalance model D200 by CAHN Instrument was used. This has an accuracy of 0.1 μg.

Computational Details for the Normal Coordinate Analysis (NCA). In order to reduce the computational problem to a tractable size, a suitable model compound was chosen to mimic the behavior of the proton acceptor. In view of the spectroscopic evidence, attention was focused onto the N-substituted imide moiety, thus selecting *N*-phenylphthalimide (NPP), whose optimized structure is represented in Figure 2.

A preliminary analysis of the molecular geometry of NPP was carried out by a molecular mechanics optimization (MM+ force field[36]), followed by a conformation searching analysis to explore in more detail the potential energy surface around the dihedral angle between the imide and the phenyl planes. The resulting structure, displaying a dihedral angle of 133.58° was used as the starting point for an ab initio calculation at the MP2 level of theory, using the 6-31G(d) basis set. The choice of this particular model chemistry was dictated by its reliability in both geometry optimization and frequency calculations for up to medium-sized systems and represented the best compromise between accuracy and computational cost. The isolated H_2O molecule was optimized by the same method prior to being merged with NPP for the analysis of the H-bonding interaction. The geometry and energetics of the NPP−H_2O aggregate were computed at the same level of theory and with the same basis set. The starting point structure was prepared by manually locating the two interacting molecules in a position such that the H atom of the proton donor and the acceptor atom were at a distance less than 3 Å and the H_2O molecule was coplanar with the phthalimide ring. Then a geometry optimization was performed, followed by a full normal coordinate analysis (NCA).[38] The latter comprises the calculation of the Hessian matrix (**F**) by determining the first and the second derivatives of the potential energy with respect to the Cartesian displacement coordinates. Both derivatives were computed analytically. The **F** matrix was then transformed in terms of mass-weighed coordinates and diagonalized to obtain the corresponding eigenvalues (normal frequencies) and eigenvectors (displacement vectors, **L** matrix). Finally, a transformation into a set of redundant internal coordinates of both the **F** and **L** matrices was accomplished in order to characterize the normal modes in terms of their potential energy distribution (PED), expressed, in normalized form, as[37,38]

$$(\mathrm{PED})_{jk} = \frac{F_{jj}L_{jk}^{\ 2}}{\sum_i FiiL_{ik}^{\ 2}} \times 100$$

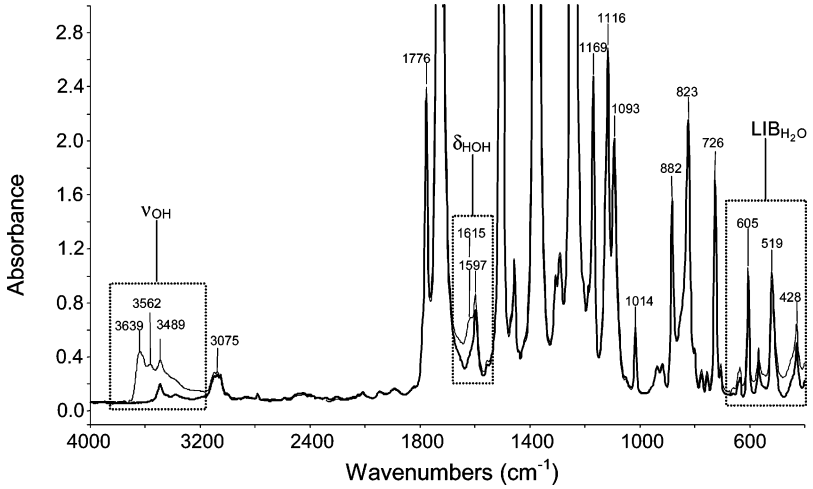

Figure 3. FTIR spectra in the 4000−400 cm^{-1} range for the polyimide film in the dry state (thick trace) and after equilibration at $a_w = 0.4$ (thin trace). Sample thickness = 20 ± 0.5 μm.

where the PED (in %) refers to the contribution of the *j*th internal coordinate to the *k*th normal mode, F_{jj} is the *j*th diagonal Force constant, and L_{jk} is the corresponding element of the **L** matrix. To compare the computed frequencies with those obtained experimentally, the set of calculated values was scaled by a factor of 0.9434, as prescribed by Wong et al.[39]

The IR intensity (in km mol^{-1}) of the normal modes was computed according to[37]

$$I_k = \frac{1}{4\pi\epsilon_0}\frac{N_A\pi}{3c^2}\sum_g\left|\frac{\partial\mu}{\partial Q_k}\right|^2 = 974.863\sum_g\left|\frac{\partial\mu}{\partial Q_k}\right|^2$$

where the summation is extended over the components of the degenerate vibration, where appropriate, and the dipole derivatives are expressed in units of $eu^{-0.5}$.

The calculations were performed on a HP system model Integrity rx2620, equipped with two parallel Itanium processors. Typical CPU times were 23 and 40 h for the isolated NPP molecule and the NPP−H_2O aggregate, respectively.

The MM module of the programs' suite Hyperchem Pro6, from Hypercube Inc. (FL), was used for the molecular mechanics (MM) calculations. For the QM and NCA calculations, the program Gaussian 03[40] (Gaussian Inc., Pittsburgh, PA) was utilized, along with its graphic interface Gaussview. The latter served to visualize the normal modes either in terms of atomic displacements or as animated vibrations, for assignment purposes.

Results and Discussion

1. Analysis of the Time-Resolved Spectra (Absorbance and Difference Spectra). In Figure 3 are reported the FTIR spectra of a completely dry polyimide film (trace A) and of the same film after equilibration with water vapor at $a_w = 0.4$ (trace B). Sorbed water displays characteristic bands in three different regions of the spectrum, i.e., in the 3650−3050 cm^{-1} range (O−H stretching modes, ν_{OH}), at around 1615 cm^{-1} (in-plane deformation, δ_{HOH}), and as a very broad absorption centered at around 500 cm^{-1} (libration modes, i.e., hindered rotation of the H_2O molecule).

Elimination of the interference from the matrix spectrum, by means of subtraction analysis (see experimental) allows us to isolate the spectrum of sorbed water in the regions of interest. The difference spectra relative to the stretching and bending modes, as collected at different times during a typical sorption experiment ($a_w = 0.4$), are reported, respectively, in spectra A and B of Figure 4. The experimental profiles are highly reproducible in both frequency ranges and are quite complex, thus suggesting the concurrent presence of various water species

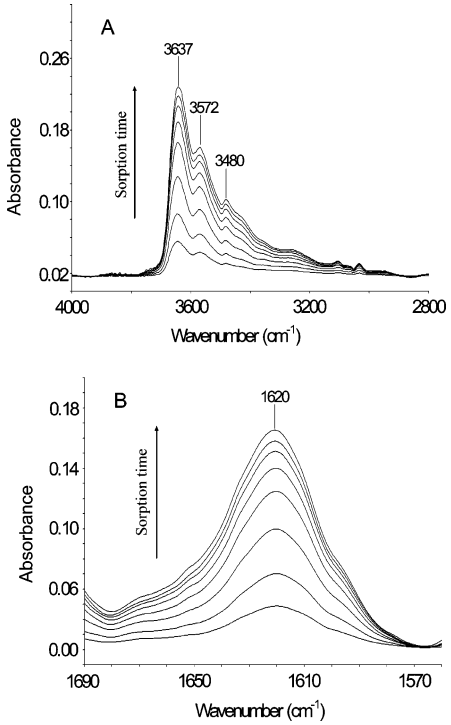

Figure 4. Difference spectra (wet − dry) collected at increasing times during the sorption experiment of H_2O vapor into the polyimide film ($a_w = 0.6$, $T = 30$ °C). Collection time increases as indicated by the arrow. (a) 4000−2800 cm^{-1} interval; (b) 1690−1560 cm^{-1} interval.

into the system. In particular, the ν_{OH} region, which is considerably more resolved, displays distinct maxima at 3637, 3572, and 3480 cm^{-1}. It turns out that the feature at 3480 cm^{-1} is not an actual maximum but rather a derivative-type feature appearing in the difference spectrum as a consequence of the downward shift of the 3490 cm^{-1} peak of the polyimide after water sorption (see spectrum of the dry polyimide, Figure 3, thick trace). This peak is a combination mode of the stretching fundamentals of the imide carbonyls ($\nu_{iph} + \nu_{ooph}$), and the shift reflects the occurrence of a H-bonding interaction. More on this later.

A curve fitting analysis of the ν_{OH} profile has been therefore attempted neglecting the above effect; the results are presented in Figure 5. These will be interpreted in detail in a following section, on the basis of the additional information gathered from 2D-FTIR spectroscopy and from the analysis of the carbonyl region of the polyimide spectrum.

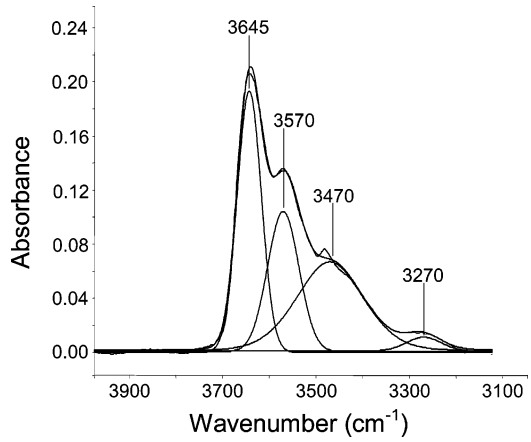

Figure 5. Curve fitting analysis of the spectrum representative of water sorbed at equilibrium ($a_w = 0.4$) in the polyimide film. The figure displays the experimental profile, the best-fitting curve and the four resolved components.

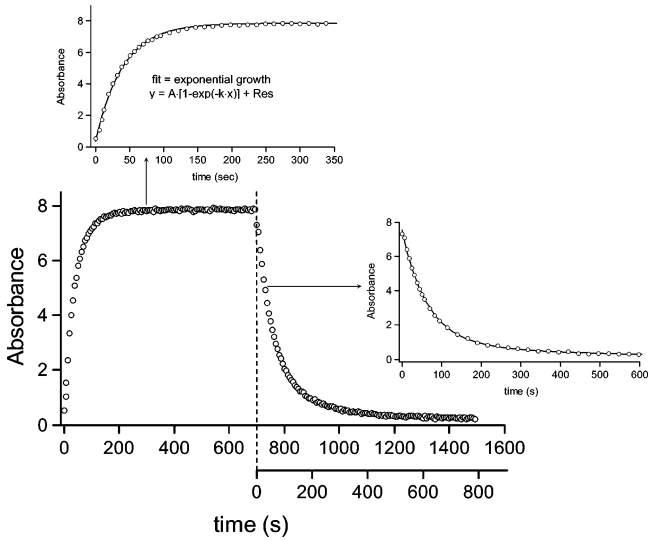

Figure 6. Absorbance of the ν_{OH} band of sorbed water as a function of time for a sorption−desorption cycle carried out on a polyimide film at $a_w = 0.4$. The two inserts display the curve fit of the experimental data points in the early part of the process by an exponential growth function for sorption and by a biexponential decay function for desorption.

Spectroscopic data as those displayed in Figure 4A,B, afford the precise monitoring of the diffusion kinetics. A typical example of a sorption−desorption cycle, as followed by measuring the absorbance area in the ν_{OH} region, is shown in Figure 6. In Figure 7, the same data are plotted in a Fick's diagram, i.e., as the ratio of absorbance at time t over absorbance at equilibrium versus the square root of time. Figure 7 evidences the Fickian behavior of the system, in agreement with previous literature reports,[14,15,41,42] and indicates that desorption is slightly slower than sorption. This result is confirmed at all investigated activities and points to a concentration dependence of the diffusivity, D (i.e., D increases by enhancing the penetrant concentration[43]). The comparative analysis of the two signals produced by penetrant molecules, as demonstrated in Figure 8, allows us to cross-check the reliability of the quantitative analysis and to confirm a linear relationship between absorbance and concentration for both signals. This linear relationship is further demonstrated in Figure 9, where the intensity of the δ_{HOH} band, normalized for film thickness, is reported as a function of the concentration of water in the sample as evaluated gravimetrically. The straight line passing through the origin

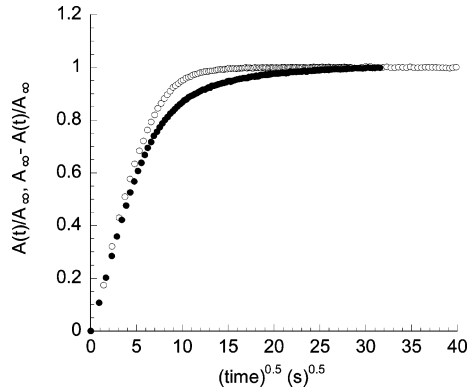

Figure 7. Sorption (○) and desorption (●) kinetics evaluated spectroscopically from the absorbance area of the H_2O band in the ν_{OH} region for a polyimide film at $a_w = 0.4$. Data represented in a Fick's diagram.

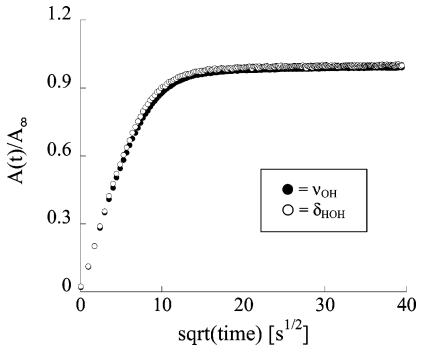

Figure 8. Sorption kinetics monitored spectroscopically for a polyimide film at $a_w = 0.4$. The quantitative analysis has been performed on the ν_{OH} band (●) and the δ_{HOH} band (○) of sorbed water.

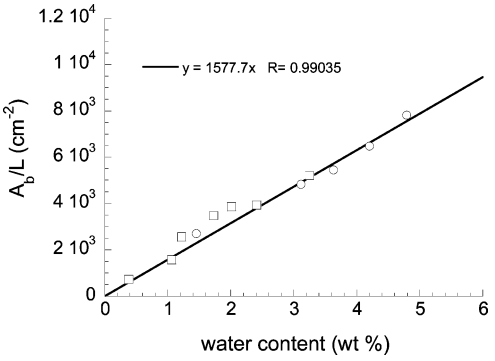

Figure 9. Calibration curve for the δ_{HOH} band of water obtained by plotting the absorbance area of the band normalized for the film thickness as a function of the concentration of sorbed water as evaluated gravimetrically. The symbols refer to two samples having different thickness: □ = 20 ± 0.5 μm; ○ = 25 ± 0.5 μm.

confirms that the system obeys the Lambert−Beer relationship, allowing direct conversion between spectroscopic and gravimetric data. The diffusion coefficients, as conventionally evaluated from the linear part of the Fick's diagrams, and the water uptake at equilibrium are reported in Table 1.

2. Two-Dimensional Correlation Spectroscopy. In order to deepen our interpretation of the spectroscopic data, it is advisable to rely on a technique which could improve the resolution and, at the same time, provide information about the dynamics of the evolving system. One of such techniques is 2-D FTIR spectroscopy, a recently developed approach based on classical time-series analysis.[44] In essence, this is a perturbation-based method in which a system, initially at equilibrium, is perturbed by an external stimulus and its response, in terms of variation

Table 1. Diffusion Coefficients and Equilibrium Water Content for the Sorption Tests Performed at Different Water Vapor Activities on a Polyimide Film Having a Thickness of 20.0 μm

H_2O activity	D ($cm^2\ s^{-1}$)	C_{H_2O} (wt %)
0.1	5.6×10^{-9}	0.41
0.2	6.5×10^{-9}	1.06
0.3	7.2×10^{-9}	1.30
0.4	8.1×10^{-9}	1.65
0.5	7.3×10^{-9}	2.04
0.6	8.1×10^{-9}	2.41
0.75	7.9×10^{-9}	3.25

of spectroscopic signals, is analyzed. On the spectral response of the system, a correlation analysis is performed, by which one measures the covariance of two variables (spectral intensities, in the case at hand) as they evolve as a function of a third common variable related to the perturbing function (time, in the present case).

Thus, the complex cross-correlation function between dynamic spectral intensities at wavenumbers υ_1 and υ_2 can be expressed as[45−47]

$$\Phi(\nu_1,\nu_2) + i\Psi(\nu_1,\nu_2) = \frac{1}{\pi T}\int_0^\infty \tilde{Y}(\upsilon_1,\omega)\tilde{Y}^*(\nu_2,\omega)\,\mathrm{d}\omega \quad (4)$$

In the above equation, $\Phi(\nu_1,\nu_2)$ is the synchronous spectrum, $\Psi(\nu_1,\nu_2)$ is the asynchronous spectrum, $\tilde{Y}_1(\omega)$ represents the forward Fourier transform (FT) of the dynamic spectral intensity $\tilde{y}(\nu_1,t)$, i.e.,

$$\tilde{Y}(\nu_1,\omega) = \int_{-\infty}^{\infty} \tilde{y}(\nu_1,t)\mathrm{e}^{-i\omega t}\,\mathrm{d}t \quad (5)$$

and $\tilde{Y}_2^*(\nu_2,t)$ is the conjugate of the FT of the dynamic spectral intensity $\tilde{y}(\nu_2,t)$, that is

$$\tilde{Y}_2^*(\nu_2,t) = \int_{-\infty}^{\infty} \tilde{y}(\nu_2,t)\mathrm{e}^{i\omega t}\,\mathrm{d}t \quad (6)$$

If the response function of the system has a well defined form, it is possible to directly derive the expression for the corresponding 2-D correlation spectrum in a closed analytical form.[45−47] This provides further insight into the significance of the linear and nonlinear correlations between the variables, as revealed by 2-D analysis.

As demonstrated in Figure 6, the dynamic component of the response function of the investigated system, $\tilde{y}(\nu,t)$ is an exponential decay of the form

$$\tilde{y}(\nu,t) = \begin{cases} \tilde{y}(\nu,t) = A(\nu)\mathrm{e}^{-k(\nu)t} & \text{for } t \geq 0 \\ 0 & \text{otherwise} \end{cases} \quad (7)$$

where $A(\upsilon)$ is the initial absorbance value and $k(\upsilon)$ is the rate constant for the signal at wavenumber υ. Applying eq 4 to such a situation, we arrive at

$$\Phi(\nu_1,\nu_2) = \frac{A(\nu_1)A(\nu_2)}{T}\frac{1}{k(\nu_1)+k(\nu_2)} \quad (8)$$

$$\Psi(\nu_1,\nu_2) = \frac{A(\nu_1)\,A(\nu_2)}{\pi T}\frac{\ln k(\nu_2) - \ln k(\nu_1)}{k(\nu_1)+k(\nu_2)} \quad (9)$$

and, if the two signals at ν_1 and ν_2 have relatively similar decay constants, eq 9 further simplifies to[26]

$$\Psi(\nu_1,\nu_2) = \frac{2A(\nu_1)A(\nu_2)}{\pi T}\frac{k(\nu_2) - k(\nu_1)}{k(\nu_1)+k(\nu_2)} \quad (10)$$

Equations 8−10 clarify the meaning of the synchronous and asynchronous spectra in the case of an exponential decay response function. In the synchronous spectrum [$\Phi(\nu_1,\nu_2)$] a peak will appear at coordinates (υ_1,υ_2) whenever there are two peaks located at υ_1 and υ_2 undergoing intensity changes during the sampling interval, irrespective of their rate constants. The synchronous spectrum is symmetric [i.e., $\Phi(\nu_1,\nu_2) = \Phi(\nu_2,\nu_1)$] and consists of autopeaks located along the main diagonal (i.e, at coordinates ν_i, ν_i) and cross-peaks appearing at off-diagonal positions. The autopeaks identify the signals that undergo changes during the experiment. They are always positive, and their intensity can be considered as a measure of the susceptibility of the relative signals to the external stimulus.[45,46] The cross-peaks, on the other hand, are positive if the two signals change in the same direction (they both increase or decrease) and are negative otherwise. It appears from the above that, in this specific case, the synchronous spectrum is relatively less interesting than the asynchronous since any changing feature produces a correlation intensity, with no specificity and limited gain in resolution.

Conversely, the asynchronous correlation spectrum [$\Psi(\nu_1,\nu_2)$] identifies decay processes having different rates as a result of the term $\ln k(\nu_2) - \ln k(\nu_1)$ or $k(\nu_2) - k(\nu_1)$, which assumes nonzero values only if the rate constants for the decay processes at the two wavenumbers are different.[45,46] This effect is responsible for the resolution enhancement of the asynchronous spectrum. It contains no autopeaks but only cross-peaks at off-diagonal positions and is antisymmetric [i.e., $\psi(\nu_1,\nu_2) = -\psi(\nu_2,\nu_1)$]. The intensity of an asynchronous peak increases as the difference between the decay rates of the relative signals increases. From eq 10, it also emerges that an asynchronous cross-peak located at coordinates (ν_1,ν_2) is positive if the intensity change at ν_1 is accelerated with respect to that at ν_2 and is negative otherwise. This is verified whenever $\Phi(\nu_1,\nu_2) > 0$. The opposite occurs if $\Phi(\nu_1,\nu_2) < 0$.[44−46]

This set of rules, often referred to as Noda's rules, is of general validity and can be reliably applied to any response function for gaining information about the sequential order of events, as long as the variation pattern of spectral intensities is reasonably monotonic during the observation period.[26,44−46]

In Figure 10A is reported the synchronous spectrum obtained from the correlation analysis of the sequence of spectra collected during the sorption test at $a_w = 0.3$. The correlation map does not provide significant enhancement of resolution, displaying only a broad maximum centered at [3635−3635 cm^{-1}], with wings at around [3450−3600 cm^{-1} (+)]. The maximum corresponds to the position of the principal water peak, which is the feature changing to the larger extent during the experiment, while the wings originate from the correlation intensity. As anticipated by inspection of the relevant equations, in the present case the synchronous correlation map is not particularly significant, due to the absence of specificity.

Many more details are evident in the asynchronous spectrum reported in Figure 10B. Here four cross-peaks are evident, centered, respectively, at [3616−3660 cm^{-1} (−)], [3570−3616 cm^{-1} (+)], [3456−3660 cm^{-1} (−)], and [3456− 3570 cm^{-1} (−)]. Asynchronous correlation is absent at 3660−3570 cm^{-1} and at 3616−3456 cm^{-1}. Thus, the overall pattern points to the presence of two couples of signals at 3660−3570 cm^{-1} and at 3616−3456 cm^{-1}; the two components of each couple change at the same rate, but the two couples exhibit different dynamics.

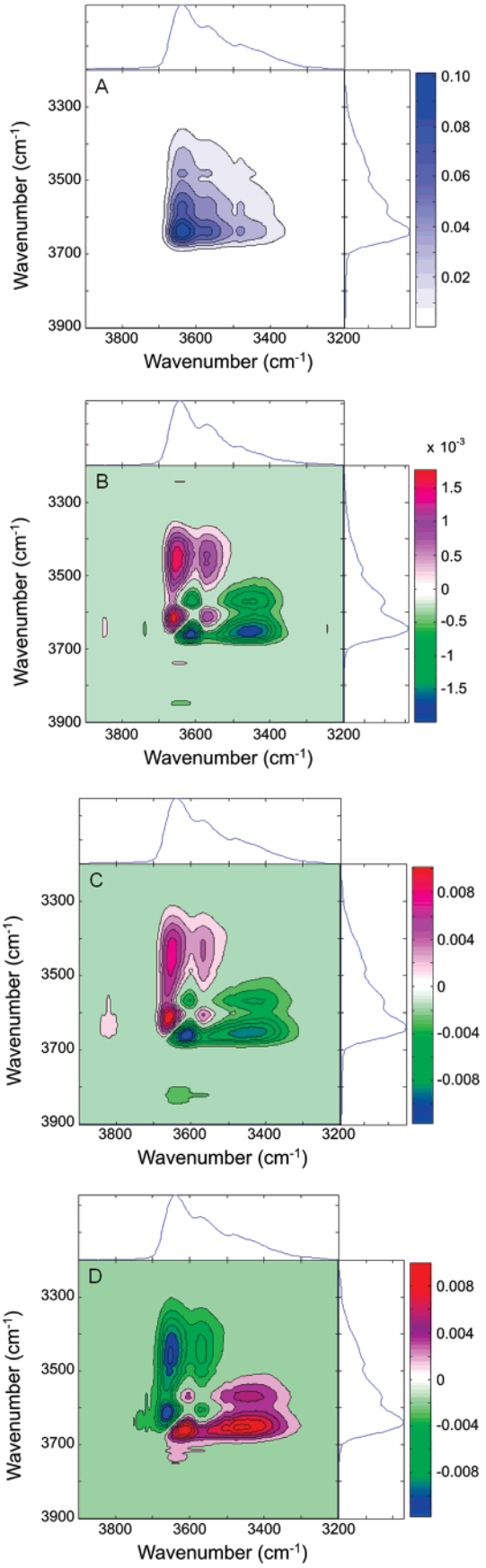

Figure 10. 2D-FTIR correlation spectra obtained by the analysis of the spectra collected during sorption/desorption experiments on the polyimide film: (A) synchronous spectrum relative to the sorption test at $a_w = 0.3$; (B) asynchronous spectrum for the sorption test at $a_w = 0.3$; (C) asynchronous spectrum for the sorption test at $a_w = 0.6$; (D) asynchronous spectrum for the desorption test at $a_w = 0.6$.

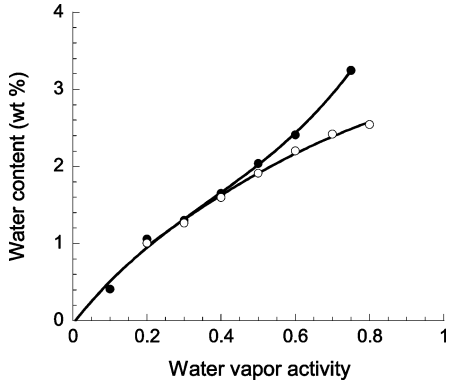

Figure 11. Water sorption isotherms for two polyimide films of different thicknesses. (●) 20 μm, data from gravimetric measurements; (○) thickness = 2.4 μm, data from FTIR spectroscopy measurements.

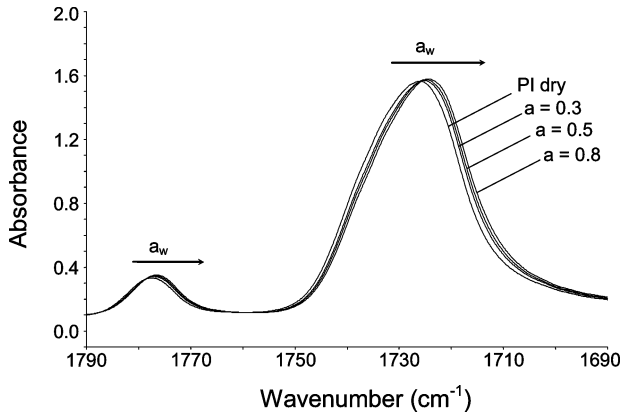

Figure 12. The carbonyl region of a polyimide spectrum (thickness 2.4 μm) in the dry state and equilibrated at different water vapor activities.

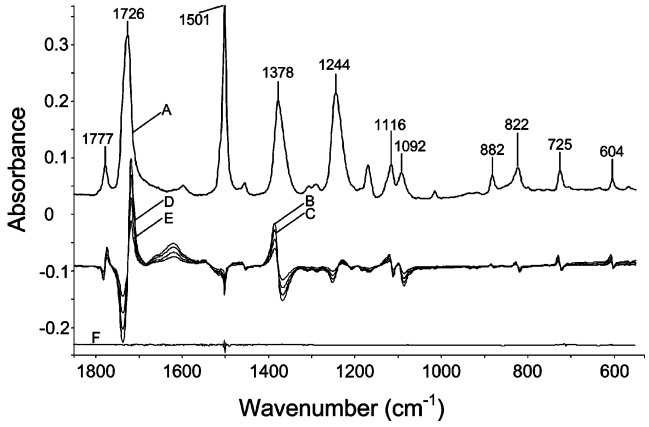

Figure 13. Trace A, FTIR spectrum in the 1850−500 cm^{-1} range for the polyimide film in the dry state. Traces B−E refer to the difference spectra obtained by subtracting the spectrum of the dry film from those of the film equilibrated, respectively, at $a_w = 0.3$, 0.4, 0.6, and 0.8. Trace F shows the spectrum of the sample after the sorption−desorption cycle at $a_w = 0.8$ minus the spectrum of the initial dry sample. The absorbance scale refers to the difference spectra. The scale of the polyimide spectrum has been reduced by a factor of 6 to facilitate the comparison.

The more straightforward interpretation of the above results is to assume the occurrence of two water species, each producing two distinct peaks. Alternative hypotheses could be put forward if one considers that species strongly bound through molecular interactions may share the same dynamic behavior. In the present case, however, the two-species hypothesis is appealingly simple,

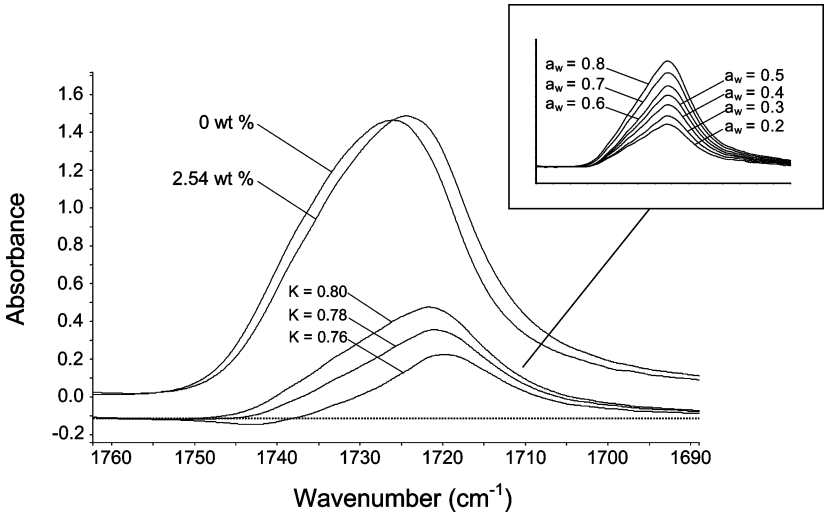

Figure 14. Subtraction analysis of the main carbonyl band of the polyimide film containing 2.54 wt % of absorbed water (see text for details). The insert displays the difference spectra obtained for the sample equilibrated at the indicated values of water vapor activity (a_w).

insofar as water molecules, in whatever environment, give rise to two stretching vibrations (in-phase at lower frequency and out-of-phase at higher frequency).

The asynchronous spectrum is very close at all investigated activities (compare Figure 10B for $a_w = 0.3$ and Figure 10C for $a_w = 0.6$). However, an interesting effect is noticed when comparing the asynchronous map relative to the sorption process (Figure 10C) and the same map obtained by analysis of the spectra collected during desorption (Figure 10D). The overall pattern is exactly coincident in the two cases but with the sign reversed. On the basis of the sign of the asynchronous peaks, we conclude that in the sorption experiment the couple of signals at 3660−3570 cm^{-1} increases faster than the two peaks at 3616−3456 cm^{-1}, while on desorption, the opposite occurs.

An attempt to elucidate the nature of the above species has to rely on the identification of the active sites on the polymer backbone and is therefore deferred after the analysis of the polyimide spectrum.

3. Identification of the Interaction Site on the Polymer Backbone and Evaluation of the Interacting Species Population. In order to recognize the site of interaction on the polymer backbone, we need to investigate the perturbation of the polyimide spectrum induced by the presence of absorbed water. In particular, we are interested in analyzing the behavior of the intense C═O stretching peaks as a function of water uptake. The samples used for diffusion kinetics were unsuitable for this purpose since for films 20−30 μm thick, both signals are above the saturation threshold (see Figure 3). The analysis requires film thickness between 1.0 and 3.2 μm, which were prepared ad hoc by a spin-coating process (see experimental). These films reach water vapor saturation in a few seconds, making kinetic data unreliable and allowing only equilibrium measurements to be considered. Two water sorption isotherms are reported in Figure 11; one of them is relative to a thin polyimide film (2.4 μm), and the concentration of sorbed water was evaluated by use of the calibration curve of Figure 9; the other curve is relative to a thicker film (20 μm), and the amount of sorbed water was evaluated gravimetrically. The two curves, essentially coincident up to $a_w = 0.4$, gradually diverge at higher activity values, which points to an influence of the film thickness on the sorption properties. This effect, already mentioned in the literature,[17,42] has not been investigated further in the present context.

A comparison between the spectra of dry and water-containing samples clearly evidences a shift of both carbonyl stretching peaks toward lower wavenumbers. This effect is shown in Figure 12, where it is also demonstrated that the shift is an increasing function of the water content in the sample. The desorption tests indicate that the effect is fully reversible, i.e., the polyimide peaks revert to their original position upon complete removal of the sorbed water (see Figure 13, trace F).

In light of the above evidence, we conclude that the imide carbonyls are the proton-accepting groups to which water molecules are bound. The molecular interaction thus established is responsible for the lowering of the carbonyl force constant (decrease of bond order) and the consequent drop of the peak frequency. The magnitude of the shift as determined from the experimental spectra without further analysis, is relatively modest, being equal to 0.86 cm^{-1} for the in-phase mode (ν_{iph}) and to 1.65 cm^{-1} for the out-of-phase mode (ν_{ooph}), for a sample containing 2.54% by weight of sorbed water.

Spectroscopic effects of such a limited extent are best appreciated by difference spectroscopy; this is demonstrated in Figure 13, where are reported the difference spectra obtained by subtracting the spectrum of the dry sample from the spectra of the samples equilibrated at various water vapor activities. In the same figure is displayed the absorbance spectrum of the dry polyimide for comparison.

We recall that in a difference spectrum, first-derivative type bands displaying a minimum and a maximum at close wavenumbers are indicative of peak shifts, i.e., a frequency displacement of the peak in the sample spectrum (wet resin) with respect to the peak position in the reference spectrum (dry resin). In particular, when the negative lobe precedes the positive, that is, occurs at higher wavenumbers, the displacement takes place toward lower frequencies (red shift). The opposite is true when the negative lobe follows the positive (blue shift). Three prominent features of this kind are immediately recognized, associated, respectively, with the two carbonyl peaks at 1777 and 1726 cm^{-1} and to the 1378 cm^{-1} band. Minor but still detectable derivative profiles are also found in correspondence to the polyimide peaks at 1244, 822, 725, and 604 cm^{-1}. It is noted that the peaks at 1777, 1726, and 1244 cm^{-1} are red-shifted, while those at 1378, 822, 725, and 604 cm^{-1} are blue-shifted. The vibrational origin of the carbonyl red-shift has already been mentioned. With respect to the other shifts, we

may anticipate, at this point, that they arise because the relative normal modes contain a significant potential energy contribution from the carbonyl double-bond. In a later section an attempt will be made to rationalize the direction and extent of the peak shifts in the light of a normal vibrational analysis (NCA) of the water−imide system.

It is possible to devise a method for the evaluation of the amount of interacting groups based on the influence of the water molecules onto the stretching modes of the imide carbonyls. It is a modified version of the approach originally developed by Marechal[18,19,24] and relies on the fact that the observed shift is actually due to the occurrence of two unresolved components: one originates from the interacting carbonyls and occurs at lower frequency and the other arises from the free carbonyls absorbing at higher frequency. The resolution of the components is not achieved because their width at half-height is comparable to their separation.

The unperturbed carbonyl component is experimentally available, being coincident with the peak observed in the fully dry polyimide. The latter, therefore, can be reliably used as reference for spectral subtraction. Accordingly, we may isolate the contribution due to the interacting carbonyls by subtracting out the $\nu_{C=O}$ peak of the dry polyimide from the corresponding band observed in the water containing samples. A critical point is to identify a criterion to obtain the correct value of the subtraction factor, *K*, which contains the information about the relative concentration of the two species. The criterion is to choose the *K* factor which reduces as much as possible the experimental profile to the horizontal baseline in the high-frequency side of the band. As soon as the profile goes below the baseline, the spectrum is oversubtracted, i.e., *K* has gone beyond its true value. The application of this procedure is illustrated in Figure 14 for the case of the sample containing 2.54% by weight of water. It is apparent that 0.02 units of *K* can be readily appreciated, producing a clear negative lobe in the difference spectrum (compare the traces with *K* equal to 0.78 and 0.76). We estimate that the above uncertainty in the determination of *K* produces an accuracy in the relative concentration values higher than 5%.

The physical meaning of *K* is immediately derived from the relevant absorbance−concentration relationships:

$$A_f = \epsilon_f L C_f \tag{11}$$

$$A_b = \epsilon_b L C_b \tag{12}$$

where *A* is the absorbance area, ϵ the molar absorptivity, *L* the sample thickness, and *C* the concentration. The subscripts f and b refer, respectively, to the "free" imide groups and to the imide groups H-bonded to water molecules. In the present case, owing to the invariance of the sample thickness upon water sorption, the subtraction spectrum, A_{diff} can be expressed as

$$A_{diff} = A_s - KA_r = L(\epsilon_f C_f + \epsilon_b C_b - K\epsilon_f C_{tot}) \tag{13}$$

where A_s and A_r refer, respectively, to the absorbance of the imide peak in the sample spectrum (water saturated film) and the reference spectrum (dry film). C_{tot} is the total concentration of imide units in the sample.

The *K* factor has been chosen so as to cancel out the contribution of the noninteracting groups, a condition that can be expressed by the relationship

$$L\epsilon_f(C_f - KC_{tot}) = 0 \tag{14}$$

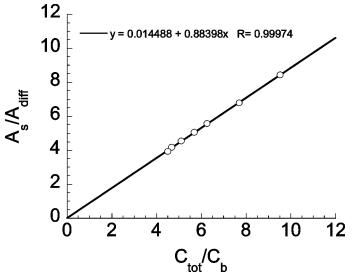

Figure 15. Absorbance ratio A_s/A_{diff} versus concentration ratio C_{tot}/C_b (see text for the meaning of the symbols). Data relative to the ν_{ooph} carbonyl band of the polyimide.

from which

$$K = \frac{C_f}{C_{tot}} \quad \text{and} \quad \frac{C_b}{C_{tot}} = 1 - K \tag{15}$$

and, combining eq 13 and 14

$$\frac{A_s}{A_{diff}} = \frac{\epsilon_f}{\epsilon_b}\frac{C_{tot}}{C_b} + 1 - \frac{\epsilon_f}{\epsilon_b} \tag{16}$$

In Figure 15, the ratio A_s/A_{diff} is reported as a function of C_{tot}/C_b, evaluated from $(1 - K)$. In accordance with eq 16, a straight line is obtained ($R = 0.9997$) with a slope of 0.88. Thus, the molar absorptivity of the bound carbonyl groups is slightly higher (1.13 times) than that of the free carbonyls, consistent with earlier literature data on C=O groups involved in H-bonding interactions. The absorptivity increase is due to an enhanced polar character of the bond involved and reflects the redistribution of the electron density caused by the proton donor. In general, the effect is proportional to the H-bonding strength and the enhancement factor can be as large as 1.5;[48] it is relatively modest in the present case, owing to the weakness of the water−imide interaction. The value of the intercept of the straight line in Figure 15 (0.014) is consistent, within the uncertainty associated with the extrapolation procedure, with the value predicted by eq 16, i.e., $(1 - 0.88) = 0.12$. The analysis described so far substantiates the quantitative method and indicates that, due to the slightly different absorptivity of the two carbonyl components, in order to quantify the concentration of the interacting groups, it is better to rely on the *K* factor than on the absorbance ratio A_s/A_{diff}.

The ratio C_b/C_{tot} can be converted into the concentration of interacting imide groups, expressed in mmol cm^{-3}, making use of stoichiometric considerations (i.e., neglecting the terminal groups' contribution and remembering that there are two imide groups per repeating unit) and from the value of the polyimide density (1.409 g cm^{-3}). The results are reported in the fourth column of Table 2. By comparison of the concentration of interacting imides with the total concentration of water molecules in the system (column 6 of Table 2), it is seen that the latter is slightly higher, as it should be, insofar as we detect, by 2D-FTIR spectroscopy, the presence of two distinct water species. The fact that the two values of C_b and C_w, obtained independently from the spectral data, are very close to each other and in the right relationship (i.e., $C_b < C_w$) at all investigated activities confirms the reliability of the quantitative analysis. It is also noticed that the percent of interacting imides over the total goes from 10% at $a_w = 0.2$ to 22% at $a_w = 0.8$, which reveals that the population of free carbonyls remains strongly predominant even at the higher activities and indicates that the possibility of a single water molecule interacting with two carbonyls is unlikely in the present system. This justifies the

Table 2. Concentration of Interacting Imide Groups Compared to the Total Concentration of Sorbed Water at the Investigated Activities, Film Thickness = 2.4 μm

a_w	K	C_b/C_{tot}[a]	C_b (mmol cm^{-3})	C_w[b] (wt %)	C_w (mmol cm^{-3})
0.2	0.895	0.10	0.77	1.00	0.79
0.3	0.870	0.13	0.96	1.27	1.00
0.4	0.840	0.16	1.18	1.60	1.25
0.5	0.824	0.18	1.30	1.91	1.50
0.6	0.804	0.20	1.44	2.20	1.72
0.7	0.786	0.21	1.58	2.40	1.88
0.8	0.778	0.22	1.64	2.54	1.99

[a] C_b, concentration of interacting imide units; C_{tot}, total concentration of imide units. [b] C_w, total concentration of sorbed water.

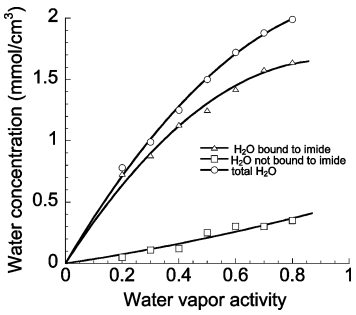

Figure 16. Total concentration of sorbed water (○), concentration of water interacting with imide carbonyls (△), and concentration of water not interacting with the imide carbonyls (□) as a function of the water vapor activity at which the samples have been equilibrated.

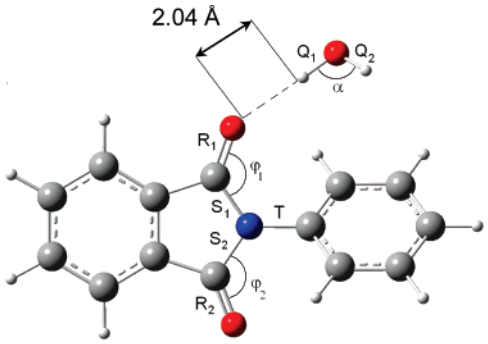

Figure 17. Optimized geometry of the *N*-phenylphthalimide−H_2O complex. For color coding and other details of the representation, see caption of Figure 2. The internal coordinates contributing to the PED of the investigated normal modes are indicated. Q, R, S, T = stretching coordinates; α, φ = in-plane bending coordinates.

assumption of a 1:1 stoichiometry for the water−imide adduct. On this basis, we are in the position to assume the concentration of the interacting water molecules to be equal to the concentration of interacting carbonyls. The quantitative analysis in terms of the two water species population is summarized Figure 16 as a function of a_w. It is seen that, in the whole activity range, the majority of H_2O molecules are interacting with the polymer substrate but the latter species decreases noticeably with the total amount of penetrant. In fact, the concentration ratio [H_2O bound to carbonyls]/[total H_2O] goes from 0.97 at $a_w = 0.2$ to 0.82 at $a_w = 0.8$.

4. Interpretation of the Vibrational Spectrum of Sorbed H_2O in the O−H Stretching Region. Having identified the interacting groups onto the polyimide backbone, we are now in the position to propose a tentative assignment for the complex profile of the water spectrum in the ν_{OH} range. We note that the main component at 3645 cm^{-1} identified by curve-fitting is further resolved, by means of 2D-FTIR analysis, in two distinct contributions at 3660 and 3616 cm^{-1}. Two other prominent peaks identified at 3570 and 3470 cm^{-1} in the curve resolved spectrum correspond to the components at 3570 and 3465 cm^{-1} in the asynchronous 2-D spectrum. Finally, a further band is found by curve fitting at 3270 cm^{-1}, with no counterparts in the 2-D spectrum, likely because of its relatively low intensity.

We propose to associate the couple of signals at 3660−3570 cm^{-1} to the out-of-phase and in-phase stretching modes of water molecules interacting with the polyimide carbonyls. The 1:1 stoichiometry of the adduct accounts for the sharpness of the two components, while their significant intensity, compared to the other peaks, finds justification in the predominance (82−97%) of this water species. The second water species produces a signal at 3616 whose FWHH is comparable to those of the components at 3660−3570 cm^{-1} and a band at 3470 cm^{-1}, which is considerably broader. This can be interpreted as a H_2O molecule interacting via H-bonding through one of its hydrogen atoms.[49−51] Thus, the stretching mode mainly localized on the "free" hydrogen would produce the sharp signal, while the vibration associated predominantly with the interacting hydrogen gives rise to the band at lower frequency, whose broadness reflects a relatively wide distribution of H-bonding distances and strengths. In view of the well-known downward shift of the ν_{OH} modes caused by the weakening of the O−H force constant upon establishment of H-bonding, we conclude that the interaction formed by the present H_2O species is stronger than that occurring with the imide carbonyls. The whole of the spectroscopic evidence points to the assignment of the peaks at 3616 and 3470 cm^{-1} to self-associated water.[51] The exact stoichiometry of this species, if any, cannot be inferred from the present data, but owing to its very low concentration (from 0.02 mmol cm^{-3} at $a_w = 0.2$ to 0.35 mmol cm^{-3} at $a_w = 0.8$), aggregates with a low monomer number (i.e., dimers, trimers) are likely to dominate. Finally, the low-intensity band identified at 3270 cm^{-1} in the curve-fitted spectrum is tentatively assigned to the first overtone of the bending fundamental, $2\delta_{HOH}$, possibly enhanced by Fermi resonance with the neighboring band at 3456 cm^{-1}.

In light of the proposed assignments, the 2-D FTIR analysis indicates that on sorption, the H_2O molecules interacting with the imide carbonyls enter the system at a faster rate with respect to self-associated water, while the opposite occurs on desorption. This interesting effect can be explained in terms of a mass-transport model based on an instantaneous, nonlinear equilibrium between the two water species, which will be discussed in detail in the second part of this contribution.

As already pointed out, the shift of the OH stretching modes is quantitatively related to the H-bonding strength, and on this ground, we may evaluate the enthalpy of formation, ΔH_0, of the H-bond between water and the interacting site of the polyimide backbone. As a first approximation, this energy can be estimated from the shift $\Delta\bar{\nu} = \bar{\nu} - \bar{\nu}_g$, where $\bar{\nu}$ is the average stretching frequency for water sorbed in the polyimide, i.e., $\bar{\nu} = ((\nu_3 + \nu_1)/2)$, and $\bar{\nu}_g$ is the same average frequency for water in the gas phase. In the above relationship, ν_3 and ν_1 refer, respectively, to the out-of-phase (antisymmetric) and the in-phase (symmetric) stretching vibrations of H_2O. However, part of this shift is due to solvation other than H-bonding; this contribution can be estimated on the basis of the Kirkwood−Bauer−Magat (KBM) relationship[52] which predicts, for inert solvents where no H-bonding with water is expected (e.g., CCl_4, CS_2, $C_2F_3Cl_3$), that $\bar{\nu} - \bar{\nu}_g \approx -120(n^2 - 1)/(2n^2 + 1)$, with n being the refractive index of the medium. Thus, taking the n

Table 3. Results of the NCA Analysis (Frequencies, Intensities, and PED) and Observed Frequencies Relative to the Normal Modes of H_2O, for the Isolated Molecule and the for the H_2O Involved in the H-Bonding Interaction with NPP

	calcd frequency (cm^{-1})	obsd frequency (cm^{-1})	% error	calcd intensity (km mol)	PED (%)	approximate description[b]
H_2O	3694	3756	1.6	39	100 Q	ν_{asym} (OH)
	3561	3657	2.6	6	100 Q	ν_{sym} (OH)
	1637	1595	2.6	89	98 α	δ (HOH)
$H_2O\cdots$NPP	3664	3660[a]	1.3	123	66 Q_1, 33 Q_2	ν_{ooph} (OH)
	3540	3570[a]	2.4	141	33 Q_1, 67 Q_2	ν_{iph} (OH)
	1660	1620	2.5	129	65 α, 15 R_1, 10 R_2	δ (HOH)

[a] From 2D-FTIR spectroscopy. [b] ν = stretching; δ = in-plane deformation. Subscript meaning: asym = antisymmetric; sym = symmetric; ooph = out-of-phase; iph = in-phase.

value for polyimide equal to 1.692, the average OH stretching frequency for unassociated water in polyimide would be 3673 cm^{-1}, while for the interacting water, $\bar{\nu} = ((3660 + 3570)/2) = 3615\ cm^{-1}$.

The difference between these values, $\Delta\bar{\nu}$, ($-58\ cm^{-1}$) measures the H-bonding energy. We may convert $\Delta\bar{\nu}$ to kilocalories for comparison with ice and for assuming a direct proportionality between the stretching frequency and the H-bond energy.[49,50,53] Knowing that, for ice, the enthalpy of formation per H-bond is approximately −6 kcal/mol[49−51] and that $\Delta\bar{\nu}$ for ice and water vapor is $3305-3707 = -402\ cm^{-1}$, we get (−6 kcal/mol)($-58\ cm^{-1}$)/($-402\ cm^{-1}$) = −0.9 kcal/mol. This value is to be compared with those reported in the literature relative to the enthalpy of formation of the H-bond between the proton-donor−proton-acceptor pairs water−acetaldeyde[54] ($\Delta H_0 = -3.6$ kcal/mol), water−dioxane[55] ($\Delta H_0 = -3.5 \pm 0.2$ kcal/mol), water−*N*,*N*-dimethylacetamide[56] ($\Delta H_0 = -3.0$ kcal/mol), water−acetone[56] ($\Delta H_0 = -2.4$ kcal/mol), and water−propylene carbonate[53] ($\Delta H_0 = -1.2$ kcal/mol). It is apparent that the ΔH_0 we have estimated for the water−polyimide system is of the same order of magnitude than those of low molecular weight analogs and is about half that of a water−ketone interaction. The result is in agreement with earlier studies reporting the polyimide carbonyls to be among the weakest proton-accepting C═O groups,[57] owing to the extensive conjugation which tends to reduce the electron density on the oxygen atom, and is consistent with the low shift values observed experimentally for the ν(C═O) vibrations (respectively, 0.86 cm^{-1} for the in-phase mode and 1.65 cm^{-1} for the out-of-phase mode).

It is well documented[49,50] that in a proton-donor−proton-acceptor pair of the type A−H···B, the shift of A−H stretching vibrations is quantitatively correlated not only with the enthalpy of H-bond formation but also with other important physical properties such as the Hammett σ function and the interbond distances. In particular, the relationship between $\Delta\nu_3$ and the A···B distance (R) has been extensively investigated.[58−60] For O−H···O systems, this dependence can be approximated by the linear relationship[60]

$$\Delta\nu_3 = 4.43 \times 10^3(2.84 - R)$$

which gives, for the system at hand, a R value of 2.81 Å. Analogously, the relationship between $\Delta\nu_3$ (in cm^{-1}) and the distance r (in Å) between the proton and the donor, i.e., A−H, can be approximated by[61]

$$r = (0.519 \times 10^{-4})\Delta\nu_3 + 0.976$$

which, from our experimental findings, gives a value of 0.983 Å. This, compared to the unperturbed value of 0.967 Å, indicates that the interaction induces an O−H bond elongation of about 2%.

5. The Theoretically Computed IR Spectrum of the Imide/H_2O Complex and Its Comparison with the Experimental Spectrum. The optimized geometry of the model compound chosen to simulate the proton acceptor, i.e., *N*-phenylphthalimide (NPP), is reported in Figure 2 (see experimental). It is noticed that the chosen model chemistry (i.e., MP2 with 6-31G(d) basis set) correctly predicts the planarity of the phthalimide ring system (within ±0.5°) while preserving the aromatic character of the two substituted benzene rings. The angle between the planes of the phthalimide unit and the phenyl ring is found to be 134.3°, while it was 133.58° in the starting-point structure. The NPP molecule has no symmetry and therefore all the 72 normal modes of vibration are predicted to be IR active. All the 72 calculated frequencies are positive; the absence of any imaginary frequency confirms that the structure obtained by the minimization process is a true minimum on the potential energy surface and not a saddle point, which is a prerequisite for the NCA approach. The complete vibrational assignment of the NPP spectrum is beyond the scope of the present work and will form the subject of a forthcoming contribution. In our analysis, we will focus on the modes involving the motion of the C═O bond, in view of the conclusions drawn from experiment which point to the involvement of the carbonyl group in the molecular interaction with H_2O.

According to the PED, the main C═O modes are predicted to occur at 1734 cm^{-1} (ν_{iph}, PED = 84% R), 1697 cm^{-1} (ν_{ooph}, PED = 85% R), and 1353 cm^{-1} (predominantly ν_{C-N}, PED = 37% T, 29% S, 7% φ). Comparison of the latter values with those observed (respectively, 1777, 1726, and 1378 cm^{-1}), shows that the average percent error, $R = ((\sum_i|\nu_i^{calcd} - \nu_i^{obsd}| \times 100)/i)$, is 2.0%, which confirms the reliability of the NCA analysis and its potential to detect the subtle interactional effects under investigation.

The optimized geometry of the NPP−H_2O complex is shown in Figure 17. The complete list of geometric parameters (i.e., bond lengths, bond angles, and torsion angles), along with the elements of the Hessian matrix, are available from the authors on request.

Here we notice that the H-bond formation causes a slight lengthening of the C═O bond involved in the interaction (from 1.222 to 1.226 Å) and a more pronounced increase of the O−H length of the proton donor (from 0.967 to 0.973 Å). The H-bonding distance (i.e., the O···H distance) is equal to 2.04 Å, while the oxygen-to-oxygen distance within the O−H···O system is 2.81 Å. These calculated values are in reasonable agreement with the experimental results (respectively, 0.983 and 3.01 Å) and are consistent with a medium to weak interaction.[49,50,59,60,61] Furthermore, it is noticed that the approaching H_2O molecule causes a decrease of the dihedral angle between the phthalimide and the phenyl rings from 134.26° in the isolated NPP molecule to 129.31° in the NPP−H_2O aggregate.

Table 4. Results of the NCA Analysis (Frequencies, Intensities, and PED) and Observed Frequencies Relative to the Normal Modes Involving the C═O Bond, for the Isolated NPP Molecule and the NPP···H_2O Aggregate

	calcd frequency (cm^{-1})	obsd frequency (cm^{-1})	% error	calcd intensity (km mol)	PED (%)	approximate description[b]
NPP	1734	1777	2.4	19	84 R	ν_{iph} (C═O)
	1697	1726	1.7	416	85 R	ν_{ooph} (C═O)
	1353	1378	1.8	498	37 T, 29 S, 7 φ	ν (CN) + δ (imide ring)
NPP···H_2O	1734	1776[a]	2.4	33	34 R_1, 50 R_2	ν_{iph}
	1693	1721[a]	1.8	459	36 R_1, 26 R_2, 24 α	ν_{ooph}
	1357	1382	1.8	461	30 (S_1 + S_2), 35 T, 7 (φ_1 + φ_2)	ν (CN) + δ (imide ring)

[a] From difference spectroscopy. [b] ν = stretching; δ = in-plane deformation. Subscript meaning: asym = antisymmetric; sym = symmetric; ooph = out-of-phase; iph = in-phase.

The parameters calculated from the NCA analysis (i.e., frequencies, PED, and intensities), along with the observed frequencies, are reported in Table 3 for the isolated H_2O molecule and for the H_2O molecule interacting with NPP. In Table 4 are summarized the same parameters relative to the normal modes of NPP involving the contribution of the C═O bond. Here again, a comparison is made between the free NPP molecule and the NPP−H_2O aggregate.

Concerning H_2O, it is seen that the calculated spectrum of the H-bonding aggregate correctly predicts a downward shift of both the stretching modes and an upward shift of the bending mode with respect to the reference state. In comparing the calculated and observed data, we have to take into account that the experimental frequencies include anharmonic contributions, while those computed are harmonic.[37,38] This will induce more pronounced effects on those modes which are highly anharmonic like the ν_{OH} vibrations. Accordingly, for these vibrations, a more meaningful comparison between theory and experiment can be made by considering the average stretching frequency (i.e., $\bar{\nu} = ((\nu_3 + \nu_1)/2)$ rather than the frequency of the single ν modes. The calculated shift, $\Delta\nu_{calcd} = \bar{\nu}_{Hb} - \bar{\nu}_f$, where the subscripts Hb and f denote, respectively, H-bonded and "free" H_2O molecules, is equal to (3602−3628) cm^{-1} = −26 cm^{-1}. On the other hand, the experimental shift is (3615−3673) cm^{-1} = −58 cm^{-1}, which indicates that the computation underestimates somehow the amount of shift, and this can be ascribed to the anaharmonicity of the vibrations involved. On the other hand, the calculated shift for the H_2O bending mode is 23 cm^{-1}, compared with an experimentally observed value of 25 cm^{-1}. The satisfactory agreement between these two values show that when the anharmonic effects are less important (as in the case of angle deformation modes), the theoretically calculated spectrum is capable of predicting not only the direction but also the amount of the frequency shift. Concerning the intensities, we observe that the predicted absolute values must be considered only approximate, while intensity ratios can be more reliably compared with experiment.[38] Thus, $(I_{Hb}/I_f)_i$, the calculated intensity ratio between the ith normal mode of bonded and nonbonded H_2O molecules, is equal to 3.2, 23.5, and 1.4 for the ν_3, ν_1, and ν_2 modes, respectively. The values relative to the ν_{ooph} and δ modes are in good agreement with literature data. In fact, for systems forming medium-to-high H-bonding interactions, absorptivity enhancements of the ν_{ooph} mode between 5 and 10 times have been reported,[49,50] while in the case of weaker interactions, the enhancement factor was found to be around 3.[23,25] The bending mode is far less sensitive to the occurrence of the interaction and its absorptivity hardly changes.[49,50] No conclusive experimental evidence has been reported for the ν_{iph} mode.

With respect to the NPP normal modes involving the C═O bond, their forms in terms of atomic displacements are reported in Figure 18. These do not differ noticeably from the atomic displacements calculated for the isolated NPP molecule. The

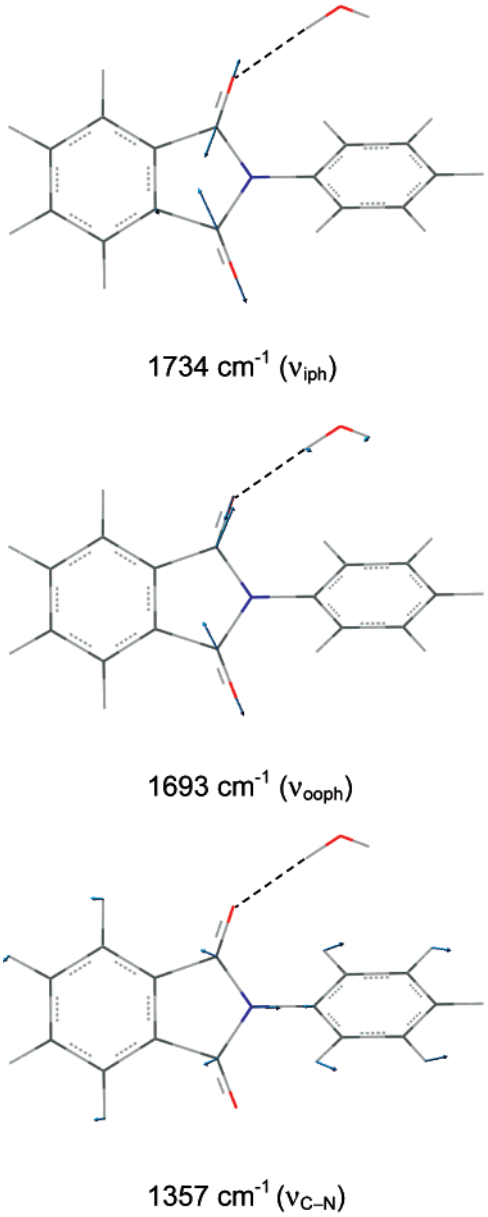

Figure 18. The form of the normal modes of NPP involving the C═O bonds in terms of atomic displacements, as calculated for the case of the NPP−H_2O aggregate.

shift computed for the ν_{ooph} mode is −4 cm^{-1}, in excellent agreement with the observed value of −5 cm^{-1}. Analogous coincidence is found for the ν_{iph} vibration (calculated −0.3 cm^{-1}, observed −2 cm^{-1}) and for the ν_{C-N} mode (calculated +4 cm^{-1}; observed +4 cm^{-1}). It is explicitly noted that this comparison is made by considering the "absolute frequency shift", i.e., the difference between the peaks of bound carbonyls as isolated by difference spectroscopy and those of "free" carbonyls as

measured in the fully dried samples. The observation that the two C═O stretching peaks are both shifted toward lower frequencies finds justification in the lowering of the carbonyl force constant, f_{R_1}, brought about by the H-bonding interaction. In fact f_{R_1} is calculated to be 0.798 mdyn/Å in the unperturbed state and 0.789 mdyn/Å in the H-bonded complex. The potential energy distribution of the ν_{C-N} normal mode reveals that the observed blue shift is to be related to the stiffening of the f_{S_1} force constant (from 0.276 mdyn/Å to 0.301 mdyn/Å) and to the increase of the f_{φ_1} force constant (from 0.143 mdyn/rad to 0.175 mdyn/rad).

Finally, it is noted that the calculated ratio $(I_{Hb}/I_f)_i$, relative to the ν_{ooph} mode is 1.1, coincident with the absorptivity ratio evaluated experimentally from the plot of Figure 15 (1.13). No experimental data are available for the intensity ratios of the other two investigated vibrations. The above results confirm the predictive capability of the adopted model chemistry for nearly harmonic vibrations and add further support to the proposed H-bonding model.

Concluding Remarks

The transport of H_2O into polyimide films has been investigated by means of time-resolved FTIR spectroscopy with the aim of elucidating the molecular mechanism of diffusion. Several approaches have been employed to analyze the spectral data, namely, difference spectroscopy, least-squares curve fitting, 2-D correlation spectroscopy, and normal coordinate analysis. The main findings of the present contribution may be summarized as follows: (i) Two distinct water species have been identified in the system, corresponding to H_2O molecules interacting with the carbonyl group of the imide moiety according to a 1:1 stoichiometry and to self-associated water, predominantly dimers and trimers. (ii) The two species display different and peculiar dynamic behaviors, i.e., on sorption, the H_2O molecules bound to carbonyls enter the system at a faster rate than the self-interacting molecules, while the opposite occurs on desorption. (iii) The enthalpy of formation, ΔH_0, of the H-bonding interaction between water and the polyimide carbonyls has been evaluated on the basis of the spectroscopic results. The ΔH_0 value of -0.9 kcal/mol was consistent with literature results and pointed to a comparatively weak H-bonding interaction. (iv) A method to quantify the population of the two water species was devised, based on the analysis of the carbonyl region of the polyimide spectrum. The analysis indicated that the vast majority of H_2O molecules (from 97 to 82%) interact at the molecular level with the polymeric substrate. (v) A normal coordinate analysis was performed on model compounds which mimic the behavior of the polyimide−water system in terms of H-bonding interactions. The IR spectrum calculated ab initio successfully predicts not only the directions but also the extent of frequency shifts for the prominent bands of both the polyimide and the water molecule in the H-bonding aggregate, especially for nearly harmonic vibrations, and adds further support to the proposed molecular models.

References and Notes

(1) Gosh, M. K., Mittal, K. L., Eds. *Polyimides: Fundamentals and Applications*; Marcel Dekker, New York, 1996.
(2) Bessonov, M. I.; Zubkov, V. A. *Polyamic Acids and Polyimides: Synthesis, Transformation and Structure*; CRC Press: Boca Raton, FL, 1993.
(3) Thompson, L. F., Willson, C. G., Tagawa, S., Eds. *Polymers for Microelectronics: Resists and Dielectrics*; ACS Symposium Series 537: American Chemical Society: Washington, DC, 1994.
(4) Feger, C.; Khojasteh, M. M.; Htoo, M. S. *Advances in Polyimide Science and Technology*: Technomic: Lancaster, PA, 1993.
(5) Roberson, L. M. *J. Membr. Sci.* **1991**, *62*, 165.
(6) Stern, S. A. *J. Membr. Sci.* **1994**, *94*, 1.
(7) Kim, T. H.; Koros, W. J.; Husk, G. R.; O'Brien, K. C. *J. Membr. Sci.* **1988**, *37*, 45.
(8) Coleman, M. R.; Koros, W. J. *J. Membr. Sci.* **1990**, *50*, 285.
(9) Mascia, L. *Trends Polym. Sci.* **1995**, *3*, 61.
(10) Wang, L.; Tian, Y.; Ding, H.; Li, J. *Eur. Polym. J.* **2006**, *42*, 2921.
(11) Hibshman, C.; Cornelius, C. J.; Marand, E. *J. Membr. Sci.* **2003**, *211*, 25.
(12) Musto, P.; Abbate, M.; Lavorgna, M.; Ragosta, G.; Scarinzi, G. *Polymer* **2006**, *47*, 6172.
(13) Thompson, L. F., Wilson, C. G., Tagawa, S., Eds. *Polymers for Microelectronics: Resists and Dielectrics*; ACS Symposium Series 537; American Chemical Society: Washington, DC, 1994.
(14) Seo, J.; Han, H. *J. Appl. Polym. Sci.* **2001**, *82*, 731.
(15) Lim, B. S.; Nowick, A. S.; Lee, K.; Viehbeck, A. *J. Polym. Sci., Part B: Polym. Phys. Ed.* **1993**, *31*, 545.
(16) Merdas, I.; Thominette, F.; Verdu, J. *J. Appl. Polym. Sci.* **2000**, *77*, 1439.
(17) Punsalan, D.; Koros, W. J. *J. Appl. Polym. Sci.* **2005**, *96*, 1115.
(18) Marechal, Y. *J. Mol. Struct.* **2003**, *648*, 27.
(19) Jamroz, D.; Marechal, Y. *J. Mol. Struct.* **2004**, *693*, 35.
(20) Cornet, N.; Beaudoing, G.; Gebel, G. *Sep. Purif. Technol.* **2001**, *22/23*, 681.
(21) Wang, Y.; Kawano, Y.; Aubuchon S. R.; Palmer R. A. *Macromolecules* **2003**, *36*, 1138.
(22) Ludvigsson, M.; Lindgren, J.; Tegenfeldt, J. *Electrochim. Acta* **2000**, *45*, 2267.
(23) Cotugno, S.; Mensitieri, G.; Musto, P.; Sanguigno, L. *Macromolecules* **2005**, *38*, 801.
(24) Marechal, Y. *J. Mol. Struct.* **1997**, *416*, 133.
(25) Mensitieri, G.; Lavorgna, M.; Musto, P.; Ragosta, G. *Polymer* **2006**, *47*, 8326.
(26) Noda, I.; Ozaki, Y. *Two-Dimensional Correlation Spectroscopy*; Wiley: Chichester, U.K., 2004.
(27) Chalmers, J. M., Griffiths, P. R., Eds. *Handbook of Vibrational Spectroscopy*; Wiley: Chichester, U.K., 2002; Vol. 2, p 935.
(28) Cotugno, S.; Larobina, D.; Mensitieri, G.; Musto, P.; Ragosta, G. *Polymer* **2000**, *42*, 6431.
(29) Mensitieri, G.; Cotugno, S.; Musto, P.; Ragosta, G.; Nicolais, L. Transport of Water in High T_g Polymers: A Comparison Between Interacting and Non-Interacting Systems. In *Polyimides and Other High Temperature Polymers: Synthesis, Characterization and Applications*; Mittal, K. L., Ed.; VSP Publishers: Leiden, The Netherlands, 2003; Vol. 2.
(30) Koenig, J. L. *Adv. Polym. Sci.* **1984**, *54*, 87.
(31) Marquardt, D. W. *J. Soc. Ind. Appl. Math.* **1963**, *11*, 441.
(32) Meier, R. J. *Vib. Spectrosc.* **2005**, *39*, 266.
(33) Czarnecki, M. A. *Appl. Spectrosc.* **1998**, *52*, 1583.
(34) Czarnecki, M. A. *Appl. Spectrosc.* **1999**, *53*, 1392.
(35) Noda, I. *Appl. Spectrosc.* **2000**, *54*, 994.
(36) Allinger, N. L. *J. Am. Chem. Soc.* **1977**, *99*, 8127.
(37) Wilson, E. B.; Decius, J. C.; Cross, P. C. *Molecular Vibrations*; McGraw-Hill: New York, 1955.
(38) Chalmers, J. M., Griffiths, P. R., Eds. *Handbook of Vibrational Spectroscopy*; Wiley: Chichester, U.K., 2002; Vol. 3, p 2003.
(39) Wong, M. W.; Wiberg, K. B.; Frisch, M. J. *J. Chem. Phys.* **1991**, *95*, 8991.
(40) Frisch, M. J.; Trucks, G. W.; Schlegel, H. B.; Scuseria, G. E.; Robb, M. A.; Cheeseman, J. R.; Montgomery, J. A., Jr.; Vreven, T.; Kudin, K. N.; Burant, J. C.; Millam, J. M.; Iyengar, S. S.; Tomasi, J.; Barone, V.; Mennucci, B.; Cossi, M.; Scalmani, G.; Rega, N.; Petersson, G. A.; Nakatsuji, H.; Hada, M.; Ehara, M.; Toyota, K.; Fukuda, R.; Hasegawa, J.; Ishida, M.; Nakajima, T.; Honda, Y.; Kitao, O.; Nakai, H.; Klene, M.; Li, X.; Knox, J. E.; Hratchian, H. P.; Cross, J. B.; Adamo, C.; Jaramillo, J.; Gomperts, R.; Stratmann, R. E.; Yazyev, O.; Austin, A. J.; Cammi, R.; Pomelli, C.; Ochterski, J. W.; Ayala, P. Y.; Morokuma, K.; Voth, G. A.; Salvador, P.; Dannenberg, J. J.; Zakrzewski, V. G.; Dapprich, S.; Daniels, A. D.; Strain, M. C.; Farkas, O.; Malick, D. K.; Rabuck, A. D.; Raghavachari, K.; Foresman, J. B.; Ortiz, J. V.; Cui, Q.; Baboul, A. G.; Clifford, S.; Cioslowski, J.; Stefanov, B. B.; Liu, G.; Liashenko, A.; Piskorz, P.; Komaromi, I.; Martin, R. L.; Fox, D. J.; Keith, T.; Al-Laham, M. A.; Peng, C. Y.; Nanayakkara, A.; Challacombe, M.; Gill, P. M. W.; Johnson, B.; Chen, W.; Wong, M. W.; Gonzalez, C.; Pople, J. A. *Gaussian 03*, revision C.02; Gaussian, Inc.: Wallingford, CT, 2004.
(41) Seo, J.; Lee, A.; Lee, C.; Han, H. *J. Appl. Polym. Sci.* **2000**, *76*, 1315.
(42) Ree, M.; Han, H.; Gryte, C. C. *J. Polym. Sci., Part B: Polym. Phys. Ed.* **1995**, *33*, 505.
(43) Crank, J. *The Mathematics of Diffusion*, 2nd ed.; Clarendon Press: Oxford, U.K., 1975.

(44) Bendat, J. S.; Piersol, A. G. *Engineering Applications of Correlation and Spectral Analysis*, 2nd. ed.; John Wiley and Sons: New York, 1993.
(45) Noda, I.; Dowrey, A. E.; Marcott, C. *Appl. Spectrosc.* **1993**, *47*, 1317.
(46) Noda, I.; Dowrey, A. E.; Marcott, C.; Story, G. M.; Ozaki, Y. *Appl. Spectrosc.* **2000**, *54*, 236A.
(47) Ekgasit, S.; Ishida, H. *Appl. Spectrosc.* **1995**, *49*, 1243.
(48) Coleman, M. M.; Painter, P. C. *Appl. Spectrosc. Rev.* **1984**, *20*, 255.
(49) Pimentel, G. C.; McClellan, A. L. *The Hydrogen Bond*; W. H. Freeman and Co.: San Francisco, CA, 1960.
(50) Murthy, A. S. N.; Rao, C. N. R. *Appl. Spectrosc. Rev.* **1968**, *2* (1), 69.
(51) Kell, G. S. In *Water and Aqueous Solutions*; Horne, R. A., Ed.; Wiley-Interscience: New York, 1972.
(52) Bauer, E.; Magat, M. *J. Phys. Radium* **1938**, *9*, 319.
(53) Cogley, D. R.; Falk, M.; Butler, J. N.; Grunwald, E. *J. Phys. Chem.* **1972**, *76*, 855.
(54) Fujiwara, Y.; Fujiwara, S. *Bull. Chem. Soc. Jpn.* **1963**, *36*, 574.
(55) Muller, N.; Simon, P. *J. Phys. Chem.* **1967**, *71*, 568.
(56) Takahashi, F.; Li, N. C. *J. Am. Chem. Soc.* **1966**, *88*, 1117.
(57) Musto, P.; MacKnight, W. J.; Karasz, F. E. *Polymer* **1989**, *30*, 1012.
(58) Rundle, R. E.; Parasol, M. *J. Chem. Phys.* **1952**, *20*, 1486.
(59) Lord, R. C.; Merrifield, R. E. *J. Chem. Phys.* **1953**, *21*, 166.
(60) Pimentel, G. C.; Sederholm, C. H. *J. Chem. Phys.* **1956**, *24*, 639.
(61) Nakamoto, K.; Margoshes, M.; Rundle, R. E. *J. Am. Chem. Soc.* **1955**, *77*, 6480.

MA071385+